Published online May 26, 2006

Resolving Structural Influences on Water-Retention Properties of Alluvial Deposits

Kari A. Winfield, John R. Nimmo,* John A. Izbicki, and Peter M. Martin

ABSTRACT

With the goal of improving property-transfer model (PTM) predictions of unsaturated hydraulic properties, we investigated the influence of sedimentary structure, defined as particle arrangement during deposition, on laboratory-measured water retention (water content vs. potential [$\theta(\psi)$]) of 10 undisturbed core samples from alluvial deposits in the western Mojave Desert, California. The samples were classified as having fluvial or debris-flow structure based on observed stratification and measured spread of particle-size distribution. The $\theta(\psi)$ data were fit with the Rossi–Nimmo junction model, representing water retention with three parameters: the maximum water content (θ_{max}), the ψ-scaling parameter (ψ_o), and the shape parameter (λ). We examined trends between these hydraulic parameters and bulk physical properties, both textural—geometric mean, M_g, and geometric standard deviation, σ_g, of particle diameter—and structural—bulk density, ρ_b, the fraction of unfilled pore space at natural saturation, A_e, and porosity-based randomness index, Φ_s, defined as the excess of total porosity over 0.3. Structural parameters Φ_s and A_e were greater for fluvial samples, indicating greater structural pore space and a possibly broader pore-size distribution associated with a more systematic arrangement of particles. Multiple linear regression analysis and Mallow's C_p statistic identified combinations of textural and structural parameters for the most useful predictive models: for θ_{max}, including A_e, Φ_s, and σ_g, and for both ψ_o and λ, including only textural parameters, although use of A_e can somewhat improve ψ_o predictions. Textural properties can explain most of the sample-to-sample variation in $\theta(\psi)$ independent of deposit type, but inclusion of the simple structural indicators A_e and Φ_s can improve PTM predictions, especially for the wettest part of the $\theta(\psi)$ curve.

A MORE COMPLETE ACCOUNTING for structural effects is critical for the development of property-transfer models that estimate unsaturated hydraulic properties, including water retention, the relation of water content (θ) to water potential (ψ), and unsaturated hydraulic conductivity $K(\theta)$, from easy-to-measure bulk physical properties. Such models typically use particle-size distribution (PSD) and bulk density (ρ_b) as their primary inputs (e.g., Gupta and Larson, 1979; Arya and Paris, 1981; Haverkamp and Parlange, 1986). Most PTMs rely on textural effects represented by the PSD. However, in many if not most soils, structural effects are at least equally important. Structure is defined as the arrangement of soil components resulting from aggregate formation, natural depositional sorting, animal burrows, shrink–swell phenomena, root channels, and similar processes.

Bouma (1989) introduced the term *pedotransfer function* to refer to the transfer of soil textural data into hydraulic data using a regression equation. We use a more general term, property-transfer model (PTM), which applies to soils and deeper sediments and to both classes of such models, empirical and quasiphysical. Empirical models rely on statistical methods to determine patterns among the bulk physical and hydraulic properties. These PTMs typically employ multiple linear regression or neural-network procedures to estimate either $\theta(\psi)$ or $K(\theta)$ from textural variables (particle-size statistics or textural-class percentages) and ρ_b. Quasiphysical models are based on theoretical physical relationships between pore sizes and particle or aggregate sizes (Arya and Paris, 1981; Haverkamp and Parlange, 1986; Nimmo, 1997; Haverkamp and Reggiani, 2002). Empirical PTMs can be further subdivided based on the specific approach chosen. One approach involves fitting a parametric $\theta(\psi)$ function (or set of functions) to the $\theta(\psi)$ measurements, and developing separate regression equations for each of the $\theta(\psi)$ parameters (Campbell, 1985; Saxton et al., 1986; Wösten and van Genuchten, 1988; Vereecken et al., 1989; Campbell and Shiozawa, 1992; Schaap et al., 1998). Another involves developing unique equations for θ at the values of ψ determined during measurement of $\theta(\psi)$ (Gupta and Larson, 1979; Rawls and Brakensiek, 1982; Puckett et al., 1985; Mecke et al., 2002). A third approach uses at least one measured value of $\theta(\psi)$, in addition to bulk physical properties, as input (Gregson et al., 1987; Schaap et al., 1998).

Measures of structure, besides ρ_b, are seldom included as input to PTMs. Arya and Paris (1981) and Haverkamp and Parlange (1986) used PSD and porosity (Φ) or ρ_b as inputs to their models, but did not include additional measures of structure. A modification to the Arya and Paris (1981) model to include aggregate-size distribution as an index of soil structure (Nimmo, 1997) improved agreement between modeled and measured $\theta(\psi)$ values by $\Delta R^2 = 12.4\%$, on average, for 17 samples tested. Nimmo (1997) also partitioned Φ into textural and structural parts approximating the fraction of Φ related to random and nonrandom aspects of structure, respectively. Qualitative structural descriptors collected as part of a soil survey—such as plasticity, stickiness, consistency, pedality, and root density—have been used in some studies for PTM development. Lin et al. (1999a) derived a system that allowed inclusion of soil structure in PTMs by assigning points to four structural categories (initial moisture state, pedality, macroporosity, and root density), in addition to texture. The final "morphometric index" varied between 0 and 1, allowing interrelations among the morphologic features to be examined. Tomasella et al. (2003), Rawls and Pachepsky (2002), and Lin et al. (1999b) found that including some measure of soil struc-

K.A. Winfield and J.R. Nimmo, U.S. Geological Survey, 345 Middlefield Road, MS 421, Menlo Park, CA 94025; J.A. Izbicki and P.M. Martin, U.S. Geological Survey, 5735 Kearny Villa Road, San Diego, CA 92123. *Corresponding author (jrnimmo@usgs.gov).

Published in Vadose Zone Journal 5:706–719 (2006).
Original Research
doi:10.2136/vzj2005.0088

Abbreviations: OG, Oro Grande; PSD, particle-size distribution; PTM, property-transfer model; SC, Sheep Creek.

ture, even if qualitative, as input to PTMs led to better predictions of $\theta(\psi)$ than if textural data were used alone.

Trapped air content at $\psi = 0$ may also serve as a structural indicator. It may be taken as A_e, the fraction of the total pore volume that remains air-filled after ψ has been raised from a negative value to 0 by typical soil-wetting processes. Maximum water contents (θ_{max}) are sometimes estimated from Φ using a rule of thumb that $A_e = 10\%$ for a typical soil (Mualem, 1974). Several researchers have measured the amount of air trapped during ponded infiltration or sprinkler irrigation tests (Fayer and Hillel, 1986; Constantz et al., 1988; Faybishenko, 1995). Fayer and Hillel (1986), in controlled water-table fluctuation tests to measure the amount and persistence of air trapping near the water table, and have observed volumetric trapped air contents (ΦA_e) ranging from 1.1 to 6.3% of the bulk soil volume. (Some authors report A_e or ΦA_e without giving Φ for converting one to the other, so it is necessary to use both quantities in reviewing past work.) The soil profile studied by Fayer and Hillel (1986) graded from a fine sandy loam at the land surface to loamy sand at 1.95 m; the maximum A_e was 13% at 0.6 m where the median particle size was approximately 0.05 mm and the uniformity coefficient was near 3.5. Constantz et al. (1988) found that A_e ranged from 4 to 19% during lab and field ponded infiltration tests. Packed columns (140 cm long) of well-sorted, commercial-grade medium sand had the largest amount of trapped air ($A_e = 19\%$, $\Phi A_e = 5\%$) in the upper 50 cm of the transmission zone. Faybishenko (1995) found that the amount of trapped air, in laboratory saturation experiments on loam-textured cores, depended on both the direction of wetting and the saturation method. Values of ΦA_e were as great as 10% by downward infiltration and <5% for upward wetting. After vacuum saturation, ΦA_e decreased to <0.2% for upward wetting. Although the results of these studies agree approximately with the $A_e = 10\%$ guideline, the materials studied typically were fine sands and loams without significant gravel content. Other researchers (Orlob and Radhakrishna, 1958; Bond and Collis-George, 1981) suggested that the amount of trapped air is related to the range of pore sizes and mean particle size, with more air trapped in materials with broad pore-size distributions and coarse texture. These observations suggest that A_e, being directly related to the particle packing, might be useful as a measure of structure.

A few laboratory studies (Croney and Coleman, 1954; Elrick and Tanner, 1955; Nimmo and Akstin, 1988; Jayawardane and Prathapar, 1992; Perkins, 2003) showed structural effects on hydraulic properties by comparing samples packed to different ρ_b values or comparing "undisturbed" samples with repacked ones. Croney and Coleman (1954) reported increases in the saturated water content of minimally expansive soils by repacking less densely. The decreased ρ_b only slightly affected the scaling parameter for water potential, ψ_o, defined such that scaling ψ by ψ_o equilibrates the ψ dependence of a set of $\theta(\psi)$ curves, and strongly steepened the rapid-drainage portion of the $\theta(\psi)$ curve. Perkins (2003) measured $\theta(\psi)$ on two deep, aggregated sediment samples in their undisturbed state and after repacking to the same ρ_b. The $\theta(\psi)$ curves for the repacked samples had smaller (more negative) ψ_o values and an increased steepness in the middle range of ψ, reflecting the destruction of macropores associated with aggregation. Other studies of repacked soil columns showed similar effects (Elrick and Tanner, 1955; Nimmo and Akstin, 1988; Jayawardane and Prathapar, 1992), in that packing reduced the heterogeneity of pore sizes, decreased the apparent ψ_o value, and steepened the drainage portion of the $\theta(\psi)$ curve.

Most PTMs available in the literature have been developed for surficial soils, often with characteristics particular to a given site and soil type, such as Lower Coastal Plain Ultisols (Puckett et al., 1985) or glacially derived Podzols (Mecke et al., 2002). Soil structural descriptors found in soil surveys (e.g., root density, plasticity, aggregate-size distribution, pedality, and stickiness) are not usually available for sediments deeper than the zone of soil development. Reliable PTMs for deeper sediments are needed, however, especially with the increasing application of unsaturated hydraulic properties to aquifer recharge and contaminant transport problems. In this study, we considered sediments that are subject primarily to a single structure-forming process, namely depositional sorting of particle sizes. This process results in relatively uncomplicated structural differences whose influence on hydraulic properties may be more systematic than other processes (e.g., biological), and may be more likely to influence both large and small pores.

The natural deposition of particles of various sizes can produce a relatively random sedimentary structure, as in a debris-flow deposit, or a more ordered structure, as in a normally graded fluvial deposit. Such a structural difference is especially relevant in applying PTMs, such as that of Arya and Paris (1981), which are applicable to sandy media and which do not account for particle arrangement. Hypothetical $\theta(\psi)$ curves are shown in Fig. 1 for an identical particle-size distribution in the two deposit types. In a normally graded fluvial deposit consisting of multiple, well-sorted (i.e., having little variation in particle size) layers with different mean particle sizes, large pores are created adjacent to the largest particles. Therefore graded fluvial samples are expected to have a wide range of pore sizes, reflected in the $\theta(\psi)$ curve by a gentler slope in the middle range of ψ. In a debris-flow deposit like that in Fig. 1, whether stratified or not, the spaces next to large particles are occupied by smaller particles and large pores are absent. At the other end of the pore-size range, no mechanism exists to make the smallest pores smaller in the debris-flow material. This deposit would thus have a narrower pore-size distribution than a fluvial deposit of identical texture. The larger pores present in normally graded fluvial deposits should cause ψ_o to have smaller magnitude than in debris flow deposits. The filling of large voids with small particles in debris flow deposits should also cause Φ, and likely θ_{max}, to be smaller than in fluvial deposits.

Our primary objective was to determine whether structural differences arising from depositional processes could be discerned in the measured $\theta(\psi)$ curves of

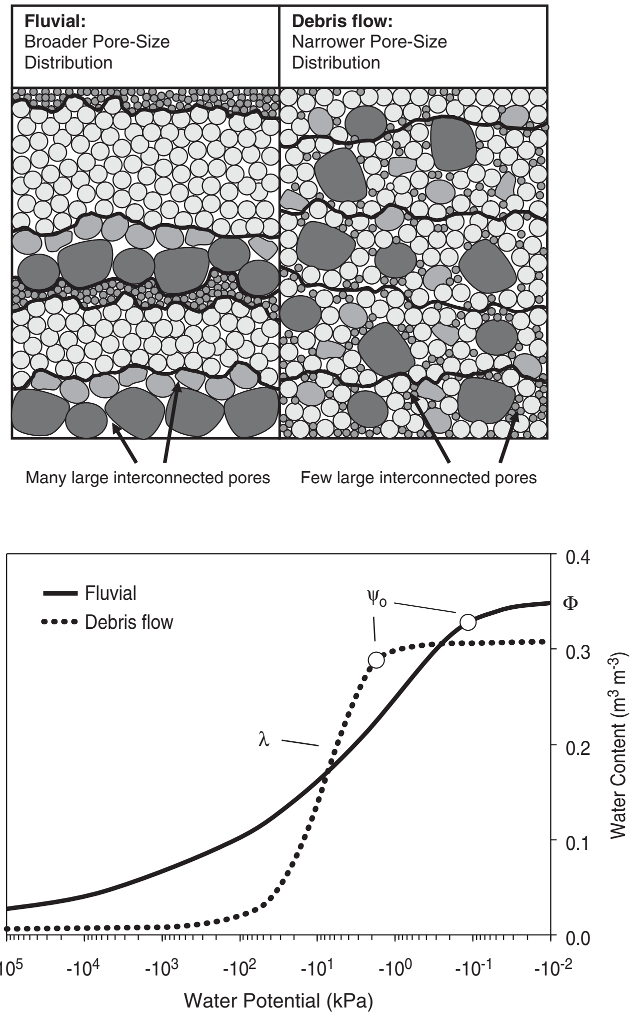

Fig. 1. Theoretical structural effects on water retention for a fluvial sample and a debris flow sample, both of which are well stratified. A fluvial sample is expected to have a broader pore-size distribution than a debris flow sample of comparable particle-size distribution because of its greater abundance of both small and large pores.

core samples. These structural differences are subtle compared with those of typical agricultural soils of mostly finer texture and significant aggregation, so that such differences are best investigated with methods of high precision and many samples. It is difficult to incorporate both of these features into a single study. In this study we emphasized the accuracy and reliability of measurements, and used several statistical techniques, subject to limitations imposed by a relatively small data set, to explore the bounds within which these types of structural differences may be significant. To investigate the relations between $\theta(\psi)$ properties and bulk physical properties of sediments with different depositional histories, we collected core samples from two washes in the Mojave Desert where both fluvial and debris-flow deposits were known to be present. Field observations near the land surface showed that one wash was dominated by fluvial deposits, the other by debris-flow deposits. Because of uncertainty about the deposit type at depth, and to treat near-surface and deep core samples on an equal basis for comparison, additional means were necessary to distinguish the characteristic depositional history of each sample, and independent indices of the degree of structural difference had to be developed.

A secondary goal, to directly quantify the degree of structural difference in the types of particle arrangement, could not be straightforwardly achieved because textural variations prevented a strict isolation of structure as an independently apparent characteristic of the available samples. Therefore additional statistical analyses were applied to texture-related and structure-related variables to achieve a similar purpose.

MATERIALS AND METHODS

Site Description and Sampling

Oro Grande (OG) Wash and Sheep Creek (SC) Wash, both part of the upper Mojave River basin of the western Mojave Desert, are ephemeral streams that drain northward from the eastern San Gabriel Mountains of the greater Transverse Range province (Fig. 2). The unsaturated zone in this area ranges in thickness from 400 m near the mountain front to 70 m toward the basin. The San Andreas Fault passes through the headwater regions of these streams along the northern margin of the San Gabriel Mountains.

The recent channel fill of OG Wash consists mainly of reworked alluvial fan deposits. The older sediments adjacent to and underlying the fill are part of the Victorville Fan Complex,

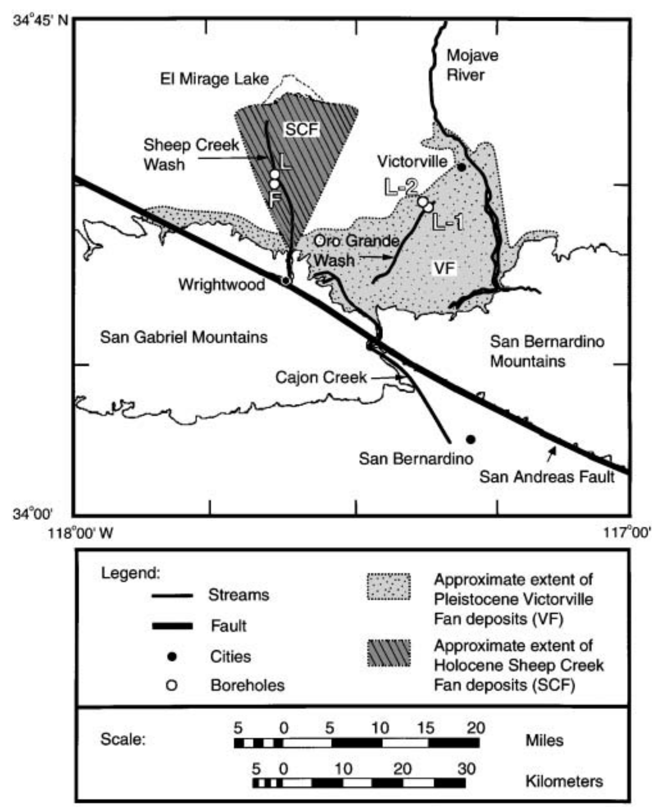

Fig. 2. Sheep Creek Wash and Oro Grande Wash and their associated fan deposits in the western Mojave Desert, San Bernardino County, California (adapted from U.S. Geological Survey, 1:250,000 San Bernardino quadrangle and modified from Weldon, 1985). Core samples were collected from the lower reaches of each wash. Boreholes L and L-1 were drilled directly in the channels, while L-2 and F were drilled into the adjacent fan surfaces.

a system of coalesced fans that were shed northward off the San Gabriel Mountains beginning about 1.5 million years ago (Weldon, 1985; Meisling and Weldon, 1989). With movement along the San Andreas Fault, headward erosion of the south-flowing Cajon Creek has beheaded the active fan complex. The source rocks for the Victorville fan deposits consist of schist, granodiorite, and sandstone, which reflect the changing source area as the southern block of the San Andreas moved northwestward (Meisling and Weldon, 1989). Because the source area has been removed by stream capture, parts of the wash have incised into the fan surface to reach the new base-level of the Mojave River, which lies about 1.5 km to the northeast of the lower part of the wash. Sediments along the channel walls near borehole L-1 (Fig. 2) appear to be dominantly fluvial in character, with abundant cross-bed sets and gravel lenses, perhaps from a braided stream environment.

SC Wash is the current trunk stream of the Holocene (Miller and Bedford, 2000) SC fan (Fig. 2), whose source area is located in the San Gabriel Mountains near the town of Wrightwood. Source rocks include a muscovite-quartz-garnet schist known as the Pelona Schist and, to a lesser degree, granite. The Pelona Schist is highly foliated and landslide-prone, and is associated with debris flows and mudflows that have affected Wrightwood (Sharp and Nobles, 1953; Morton and Sadler, 1989) and have reached as far down fan as El Mirage Lake. Along incised portions of the wash (e.g., near Borehole L, Fig. 2), deposits appear to be debris-flow dominated. The incision may have resulted from uplift of the San Gabriel Mountains during the deposition of the fan sediments.

Samples containing a broad range of particle sizes were selected for detecting structural differences of the type shown in Fig. 1. Four boreholes were drilled and core-sampled in 1994, 1995, and 1997 at the lower reaches of the washes (Fig. 2) to depths of approximately 30 m below land surface (Izbicki et al., 1995, 1998, 2000; Izbicki, 1999). Boreholes L and L-1 were drilled directly in the channels and Boreholes L-2 and F were drilled on the adjacent fan surfaces. Two borehole samples from each wash (OGL-1 11.5, OGL-2 82, SCF 57, and SCL 58) were chosen based on textural descriptions in the lithology logs (Izbicki et al., 2000) and their minimally disturbed state. (Note sample nomenclature is as follows: for borehole samples, wash abbreviation followed by borehole number and sample depth in feet; for surficial samples, wash abbreviation followed by sample number, numbered sequentially in order of collection by wash). In 1998, nine shallow core samples were collected along the incised part of each wash. Sampling criteria included apparent texture and deposit type. The collection method involved (i) creating a horizontal bench in the channel wall, (ii) placing a core liner identical to that used for borehole sampling (10-cm diameter, 15-cm length) on the resultant flat surface, and (iii) pushing the liner vertically downward as sediment was carved away from the sample base (Winfield, 2000). For most shallow samples, water was added to the core liners to aid in collection. A subset of three shallow core samples from each wash (OG-1, OG-2, OG-4, SC-1, SC-2, and SC-4) was selected based on apparent textural similarity, determined by measuring PSDs of bulk samples collected adjacent to the core sampling locations. The samples did not display significant aggregation or ped development, and there was no observable caliche, so these samples were suitable for analysis in terms of the simple structural characteristics described above and systematically illustrated in Fig. 3.

Laboratory Methods

Before measuring $\theta(\psi)$ curves, samples were wetted from the bottom upward to "natural satiation" by either (i) submerging samples in a dish filled to approximately half-height with the wetting solution or (ii) (for Samples SC-1 and OG-4) adding water incrementally using the controlled-liquid volume apparatus (Fig. 4; Winfield and Nimmo, 2002). For the submerged samples, saturation to θ_{max} was completed when sample weight no longer changed with repeated weighing. With the controlled-liquid volume apparatus, water was added in small amounts (typically 5–15 mL) until the ψ value, indicated by closing off the water supply and switching to a transducer,

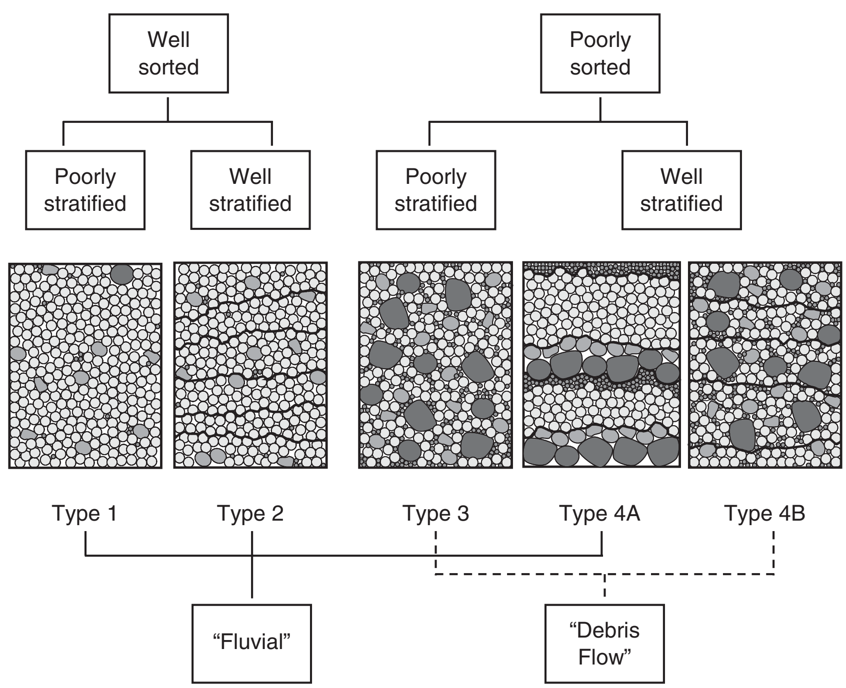

Fig. 3. Sample classification scheme, based on geometric particle-size standard deviation and stratification, used to distinguish between fluvial and debris flow sediments.

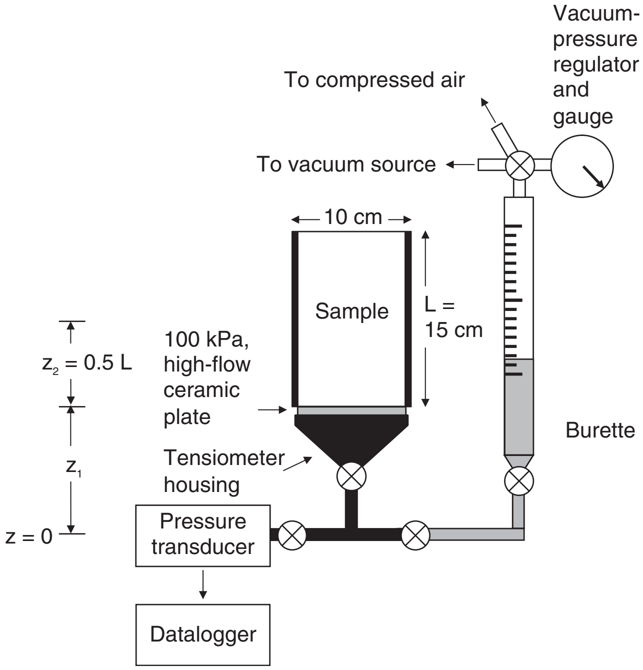

Fig. 4. Laboratory controlled-liquid volume apparatus for measuring wet- to mid-range water retention values on large, undisturbed core samples (Winfield and Nimmo, 2002).

was equivalent to about one-half the sample height. Then by either method ψ would equal zero near the midpoint of the sample. For saturating the samples and measuring $\theta(\psi)$, the wetting solution consisted of deionized water with calcium chloride ($CaCl_2{\cdot}2H_2O$) added to establish a near-natural electrolyte concentration, and sodium hypochlorite (NaOCl) added to inhibit microbial growth in the sample and ceramic pores.

Immediately after saturation, $\theta(\psi)$ curves were measured by removing water in fixed steps, and allowing the samples to reach equilibrium (ψ constant with time). For rapid and high-resolution measurement of $\theta(\psi)$ for $\psi > -50$ kPa, water was extracted using the controlled-liquid volume method (Winfield and Nimmo, 2002). Values of θ were controlled by extracting with external suction a prescribed amount of water, monitored volumetrically in a burette. After water was extracted, equilibration was initiated by closing off the burette and monitoring ψ with a transducer. For $\psi < -50$ kPa, forced evaporation of water was used to control θ, with θ determined by sample weighing and expressed volumetrically using the measured dry ρ_b of the sample. At equilibrium, for $-10\,000$ kPa $< \psi < -50$ kPa, ψ was measured by the filter paper method (Greacen et al., 1987), using Whatman (Brentford, UK) no. 42 ashless filters.[1] For $\psi < -10\,000$ kPa, additional $\theta(\psi)$ points were measured by evaporating water from small (1 to 3 g) representative splits of the samples in a desiccating chamber and immediately measuring ψ with a Decagon model CX-2 chilled-mirror hygrometer (Gee et al., 1992).

For the controlled-liquid volume and filter paper methods, core samples were kept in their original liners to minimize sample disturbance and to retain the influence of structural features. For the hygrometer method, disturbed samples were acceptable because in the dry range of $\theta(\psi)$ water coats particles as thin films, making structural influences on ψ negligible.

[1] Brand names are given to identify products used in research, and do not imply endorsement by the U.S. Geological Survey.

Bulk physical properties, including PSD, ρ_b, and particle density (ρ_s), were determined after the $\theta(\psi)$ measurements were completed. Bulk sample volume was calculated from the dimensions of the core liner after adjusting the core length to account for recesses and protrusions at the sample ends. Samples were then carefully pushed from their liners, cut in half longitudinally, and examined for stratification or other features that would allow classification of the dominant depositional mode (Fig. 3). Samples were oven dried at 105°C, and ρ_b was calculated from the oven-dry weight and bulk sample volume. Values of ρ_s were determined by the pycnometer method (Blake and Hartge, 1986), using approximately 5 g of material from the size range <0.85 mm. Values of Φ were calculated as $1 - (\rho_b/\rho_s)$. The relative abundance of particles with effective diameters (d) between 0.85 and 90 mm (for 14 particle-size intervals, or "bins") was determined by dry sieving, and between 4×10^{-5} and 0.85 mm (for 107 bins) by optical light scattering (Gee and Or, 2002) with a Coulter LS 230 Series (Beckman Coulter, Fullerton, CA) particle-size analyzer. The bin spacing, Δd, is defined as $\log_{10}(d_{upper}) - \log_{10}(d_{lower})$, where d_{upper} represents the upper and d_{lower} the lower bin limit. The average Δd changed at 0.85 mm, from 0.0404 for the optical method to 0.1446 for the dry sieve method.

Two other parameters were computed from measured data and used to evaluate structure: A_e and a porosity-based randomness index (Φ_s). The trapped-air fraction (A_e) was computed from the difference between the measured Φ and θ_{max}. A medium that has more pronounced structure in terms of greater deviation from a random arrangement of particles will in general have greater Φ. For quantitative emphasis of this effect as a departure from randomness, instead of using Φ directly, we use Φ_s, defined as $\Phi - 0.30$. The value 0.30 was chosen as a value exceeded by Φ of most granular media, and which approximates Φ for particles arranged with perfect randomness (Nimmo, 1997). Negative values of Φ_s are possible because it is a difference from an artificially fixed datum.

Representation of Water-Retention Curves

Measured $\theta(\psi)$ points were fit with the Rossi and Nimmo (1994) junction model, represented by different functions in each of three segments of the complete $\theta(\psi)$ curve:

$$\theta = \theta_{max}\left[1 - c\left(\frac{\psi}{\psi_o}\right)^2\right] \quad 0 \geq \psi \geq \psi_i \qquad [1a]$$

$$\theta = \theta_{max}\left(\frac{\psi_o}{\psi}\right)^{\lambda} \quad \psi_i \geq \psi \geq \psi_j \qquad [1b]$$

$$\theta = \theta_{max}\alpha\ln\left(\frac{\psi_d}{\psi}\right) \quad \psi_j \geq \psi \geq \psi_d \qquad [1c]$$

where ψ_d is the matric potential at which $\theta = 0$ (oven-dryness), and c, λ, α, ψ_o, ψ_i, and ψ_j are empirical parameters. This model realistically represents $\theta(\psi)$ in the driest as well as the wetter ranges. The parabolic function near saturation allows the pore-size distribution [the first derivative of the $\theta(\psi)$ curve] to be computed without a discontinuity near ψ_o.

The model includes constraints of continuity and smoothness at the junction points ψ_i, and ψ_j, which link the empirical parameters such that only two of the six, usually taken as λ and ψ_o, are independent. Sometimes ψ_o is called the "air-entry" potential, but air actually begins displacing water in the largest pores between ψ_o and 0 (Fig. 1). The λ parameter indicates the relative steepness of the middle portion of the $\theta(\psi)$ curve.

The value of ψ_d was determined based on the SSSA (1997) definition of zero water content and the Kelvin equation:

$$\psi_d = -(R/M)T_o[\ln(p_o/p_{so})] \quad [2]$$

where R/M is the ratio of the universal gas constant to the molecular weight of water (461.53 J kg^{-1} K^{-1}), T_o is the oven temperature (378 K), p_o is the vapor pressure of water in the oven, and p_{so} is the saturation vapor pressure for water at 378 K. Additional assumptions are required to estimate p_o. We assume p_o equilibrates with water vapor pressure in the lab air under typical lab conditions of 50% relative humidity and temperature at 295 K. Then, using values from standard tables (e.g., Dorsey, 1940), ψ_d equals −788 MPa. For convenience and consistency with other reports (Ross et al., 1991; Andraski, 1996; Rossi and Nimmo, 1996), $\psi_d = -1000$ MPa was used in the model fits.

Nonlinear regression to the $\theta(\psi)$ measurements, based on a modified Gauss-Newton least-squares approach, was achieved using custom-written Matlab programs (Statistics Toolbox version 3 of MATLAB 6, Release 12, The Mathworks, Inc., Natick, MA). The values of ψ_o and λ were optimized, and θ_{max} and ψ_d were fixed.

Descriptive Univariate Statistics

Because sediment PSDs typically follow lognormal distributions (Krumbein, 1938; Pettijohn, 1975), core sample PSDs were characterized using geometric particle-size statistics (geometric mean M_g and σ_g). We chose the mean rather than the median particle diameter to characterize the PSD because the mean incorporates the influence of all particle sizes, including multiple modes and skewness, on the normal distribution. Values of M_g were computed using the method of moments (Beyer, 1991):

$$\log_{10}(M_g) = \frac{\sum_{i=1}^{n}[f_i(d_{ci})\log_{10}(d_{ci})]}{\sum_{i=1}^{n} f_i(d_{ci})} \quad [3]$$

where n is the number of bins, d_{ci} is the geometric center of the ith bin (or $10^{[\log_{10}(d_{upper})+\log_{10}(d_{lower})]/2}$), and $f(d_{ci})$ corresponds to the frequency of particles occurring within the ith bin assigned to d_{ci}. Values of σ_g were calculated by:

$$[\log_{10}(\sigma_g)]^2 = \frac{\sum_{i=1}^{n}\{f_i(d_{ci})[\log_{10}(d_{ci}) - \log_{10}(M_g)]^2\}}{\sum_{i=1}^{n} f_i(d_{ci})} \quad [4]$$

Because Δd of the measured PSD changed at 0.85 mm, a slight discrepancy exists between the statistical values calculated using the unequal, measured bin sizes and the values calculated from a distribution with an equal Δd for the entire range of particle sizes. Values of M_g and σ_g calculated from the PSDs with the original, irregular bin spacing (average Δd = 0.052) were compared with those calculated from PSDs where the number of bins was reduced from 121 to 40, so that Δd was equal to 0.16 on average (approximating the Δd of the sieved particle-size fraction). The average difference between these two ways of calculating M_g was 0.005 mm, with smaller M_g resulting from the larger Δd (0.16) for all samples. The average difference in σ_g was 0.009, with smaller σ_g for about one-half of the samples. These results indicate that the change in Δd at 0.85 mm does not significantly affect the final values of M_g and σ_g. Scheinost et al. (1997) treated this problem in a similar way and also concluded that the effect of bin size was small.

RESULTS AND DISCUSSION

Hydraulic and Bulk Physical Properties

The cumulative PSDs for the 10 core samples, divided into groups by wash, are shown in Fig. 5. Bulk physical properties, including ρ_b, ρ_s, texture, textural class percentages, and geometric particle-size statistics (M_g and σ_g), are summarized in Table 1. On average, SC Wash samples had larger ρ_s than OG Wash samples because of the greater presence of heavier minerals such as garnet and muscovite (derived from the schistose source rocks). The samples contained significant gravel and ranged in texture from sandy loams to very gravelly sands according to the USDA soil classification system (Soil Survey Staff, 1975).

The $\theta(\psi)$ curves, including measured points and Rossi–Nimmo (1994) junction model fits, are shown in Fig. 6. Measured values of θ_{max}, optimized values of λ and ψ_o, and calculated values of Φ, Φ_s, maximum percentage saturation (S_e), and A_e are listed in Table 2. The trapped air fraction A_e ranged from 2.8 to 35.9%. Initial θ values (θ_{init}), determined immediately before laboratory saturation, are also given in Table 2. The six surficial samples were partially saturated in the field during their collection, so their θ_{init} values were larger. Samples with large

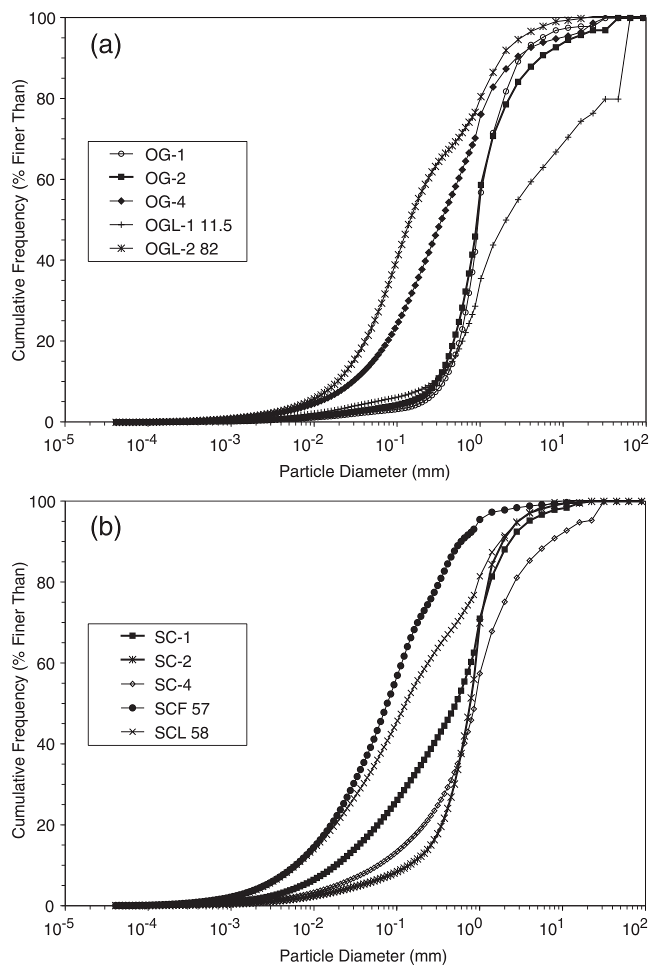

Fig. 5. Cumulative particle-size distributions for core samples collected from (a) Oro Grande Wash and (b) Sheep Creek Wash.

Table 1. Summary of core samples collected from Oro Grande (OG) Wash and Sheep Creek (SC) Wash, including depths, measured bulk (ρ_b) and particle (ρ_s) densities, USDA textural class percentages, and geometric particle-size statistics.

					Particle-size fraction (mm)				Geometric particle-size statistics	
Sample	Depth interval	ρ_b	ρ_s	Texture	Gravel (>2)	Sand (2–0.05)	Silt (0.05–0.002)	Clay (<0.002)	Mean diameter, M_g	Standard deviation, σ_g
	m	g cm^{-3}			%				mm	
OG-1	1.5–1.65†	1.73	2.79	gravelly sand	18.11	79.19	2.26	0.38	0.937	3.34
OG-2	2.4–2.55†	1.70	2.66	gravelly sand	21.38	75.29	2.83	0.48	0.962	4.29
OG-4	4.0–4.15†	1.79	2.65	loamy sand	12.65	71.76	14.16	1.47	0.304	6.92
OGL-1 11.5	3.5–3.7	1.92	2.69	very gravelly sand	50.31	44.93	4.37	0.71	2.674	9.49
OGL-2 82	25–25.2	1.83	2.79	loamy sand	8.35	66.73	23.60	1.67	0.167	6.55
SC-1	0.9–1.06†	1.88	2.77	loamy sand	11.98	69.27	17.19	1.65	0.304	7.17
SC-2	0.6–0.75†	1.67	2.77	sand	9.01	84.89	5.39	0.70	0.581	3.88
SC-4	0.6–0.75†	1.80	2.76	gravelly sand	24.80	65.84	8.45	0.89	0.711	6.72
SCF 57	17.38–17.53	1.60	2.74	sandy loam	2.32	56.70	37.11	4.05	0.068	6.38
SCL 58	17.68–17.84	1.93	2.71	sandy loam	8.68	57.03	30.66	3.86	0.119	8.88

† Approximate depth below adjacent fan surface. Samples collected along incised portions of SC Wash and OG Wash.

θ_{init} values had A_e values ranging from 7.4 to 35.9%; the initial "wet" state of these samples did not correlate with greater A_e ($r = 0.071$).

Seven of the ten A_e values exceeded the 10% guideline. In general, samples with greatest M_g had the greatest A_e values, and samples with greatest σ_g had the smallest. Samples OG-1 and OGL-1 11.5, two of the most coarsely textured samples, had the largest A_e. Sample OGL-1 11.5 contained a large gravel clast (effective diameter 53 mm, representing about 7% of the bulk sample volume) that increased M_g and σ_g. Large A_e values may also result from the difficulty in maintaining full saturation as water drains out of the samples before weighing. Unfortunately little experimental work has been done on the effect of wetting rate, which was not completely controlled in our experiments, on the amount of air trapped. Davidson et al. (1966) measured differences in satiated water content (θ_{max} after wetting) due to the related issue of wetting pressure-step size. They showed more air was trapped with larger step sizes (analogous to faster wetting), but the differences in ΦA_e were about 0.03, much smaller than the sample-to-sample differences in our measurements. Our results suggest the typical A_e guideline of 10% may be much too small for coarse-textured alluvial deposits. Expectations for generally lower A_e values may derive from the large body of published data for samples that had been sieved and repacked with gravel removed.

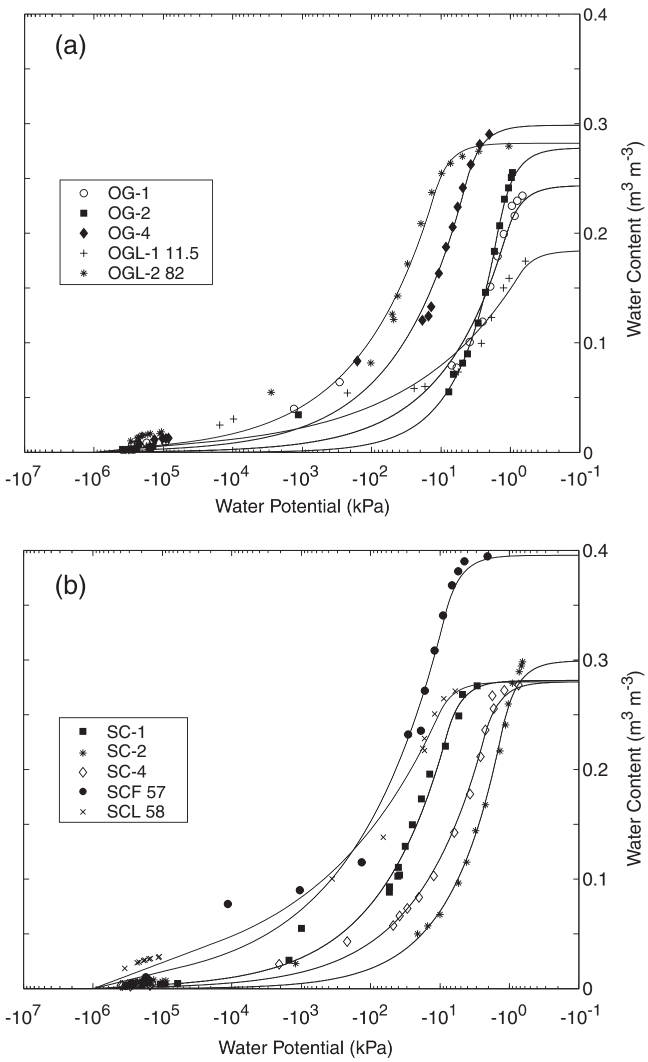

Fig. 6. Water desorption measurements and curves fitted using the Rossi–Nimmo (1994) junction model for core samples from (a) Oro Grande Wash and (b) Sheep Creek Wash.

Sample Classification According to Depositional Environment

A significant research difficulty arose from the fact that samples from OG Wash displayed debris-flow as well as the expected fluvial structural features and that the converse was true for SC Wash, preventing separation of samples into structural categories independently of observable features of the samples. Both fluvial and debris-flow facies can exist at an individual wash because of possible shifting of positions and local reworking of fan deposits. Therefore, additional means of categorizing the samples were necessary, using combinations of degree of particle-size sorting and stratification, as shown in Fig. 3.

For most samples, the degree of stratification was described by examining the core samples after $\theta(\psi)$ measurement. For Samples OG-4 and SC-1, the degree of stratification was discerned from photographs taken along the channel walls during sample collection. In general, samples with three or more visible layers in

Table 2. Summary of core-sample hydraulic properties, including initial water content, calculated total porosity, maximum saturated water content, porosity-based randomness index, trapped air fraction of porosity, and optimized water-retention parameters for the Rossi–Nimmo (1994) junction model.

Sample	Initial water content† θ_{init}	Total porosity Φ	Porosity-based randomness index‡ Φ_s	Max. water content θ_{max}	Max. saturation§ S_e	Trapped air fraction of porosity§ A_e	Scaling parameter for water potential ψ_o	Curve-shape parameter λ
	$m^3\ m^{-3}$				%		kPa	
OG-1	0.198	0.379	0.079	0.244	64.4	35.6	−0.746	0.472
OG-2	0.181	0.359	0.059	0.278	77.4	22.6	−0.997	0.770
OG-4	0.273	0.323	0.023	0.299	92.6	7.4	−2.789	0.435
OGL-1 1.5	0.061	0.287	−0.013	0.184	64.1	35.9	−0.464	0.274
OGL-2 82	0.049	0.343	0.043	0.282	82.2	17.8	−7.839	0.393
SC-1	0.276	0.321	0.021	0.281	87.5	12.5	−5.101	0.436
SC-2	0.215	0.397	0.097	0.299	75.3	24.7	−0.848	0.585
SC-4	0.074	0.350	0.050	0.280	80.0	20.0	−1.478	0.449
SCF 57	0.042	0.417	0.117	0.396	95.0	5.0	−5.335	0.325
SCL 58	0.045	0.288	−0.012	0.280	97.2	2.8	−6.504	0.241

† θ_{init} is the initial water content before saturation and does not represent the field water content.
‡ $\Phi_s = \Phi - 0.3$.
§ S_e was calculated from the relation $100(\theta_{max}/\Phi)$. A_e was then calculated as $100 - S_e$.

their 15-cm length were considered well stratified; fewer than this would mean that the sample did not capture a single complete layer.

The degree of particle-size variation within each sample was computed in terms of sorting using sedimentological units ϕ [$= -\log_2(d)$, where d = effective diameter in millimeters]. The cutoff between moderately sorted to well sorted and poorly sorted materials occurs at 1 ϕ, with $\phi < 1$ indicating better sorting (Folk, 1980). Because equivalent sorting definitions do not exist for the geometric standard deviation (σ_g), we defined the sorting criterion at $\sigma_g = 5$, which approximates a graphical particle-size standard deviation of 2ϕ. Samples with $\sigma_g < 5$ are considered here as well sorted.

Depositional environment was inferred for each type based primarily on degree of sorting. Types 1, 2, and 4A are inferred to represent fluvial materials because each type is characterized by a narrow range of particle sizes either for the entire sample or for individual layers. Types 3 and 4B are inferred to represent debris flow deposits because the range of particle sizes for each layer or for the entire sample is broad. Type 4A, with well-sorted layers, and Type 4B, with poorly sorted layers, are of most interest for determining structural effects on $\theta(\psi)$, especially for samples of comparable PSDs.

Sample classification results are presented in Table 3. Three samples were identified as fluvial (OG-1, OG-2, and SC-2) and three as debris flow (OGL-1 11.5, OGL-2 82, and SC-1). The remaining four samples could not be classified because of lack of information about sorting within individual layers (Type 4 samples) or about the degree of stratification. Thus there is not enough information to completely correlate observed structural influences as hypothesized in Fig. 1 with features of measured $\theta(\psi)$ curves. However, the degree of textural and structural influence may be inferred by comparing $\theta(\psi)$ parameters (θ_{max}, ψ_o, and λ) with the textural indicators M_g and σ_g,, and the structural indicators A_e and Φ_s.

Parameter Correlation Analysis

Correlations among the unsaturated hydraulic parameters θ_{max}, ψ_o, and λ and the indicators M_g, σ_g, ρ_b, Φ_s, and A_e are examined in Fig. 7 and 8, and quantified as correlation coefficients (r) in Table 4 for $n = 10$ samples. In this discussion, we make a number of comparisons, a few of which are supported by all or nearly all samples, whereas some are clearly less well supported as general conclusions because data were available for only three each of fluvial and debris-flow samples.

Table 3. Sample classification based on the geometric particle-size standard deviation and degree of stratification observed from the core samples after water retention measurement.

Sample	Geometric particle-size standard deviation σ_g	Number of layers†	Sorting description‡	Stratification description†‡	Type§	Inferred depositional environment¶
OG-1	3.34	8	well	well	2	F
OG-2	4.29	1	well	poor	1	F
OG-4	6.92	(ND)	poor	(ND)	3 or 4	ND
OGL-1 11.5	9.49	1	poor	poor	3	D
OGL-2 82	6.55	2	poor	poor	3	D
SC-1	7.17	(1)	poor	(Poor)	3	D
SC-2	3.88	1	well	poor	1	F
SC-4	6.72	3	poor	well	4	ND
SCF 57	6.38	8	poor	well	4	ND
SCL 58	8.88	4	poor	well	4	ND

† ND = not determined; () indicates observation made from field photographs.
‡ Well-sorted samples have $\sigma_g < 5$. Well-stratified samples have three or more layers.
§ Type refers to the unique combination of sorting and stratification description as shown in Fig. 3.
¶ *F*, fluvial; *D*, debris flow.

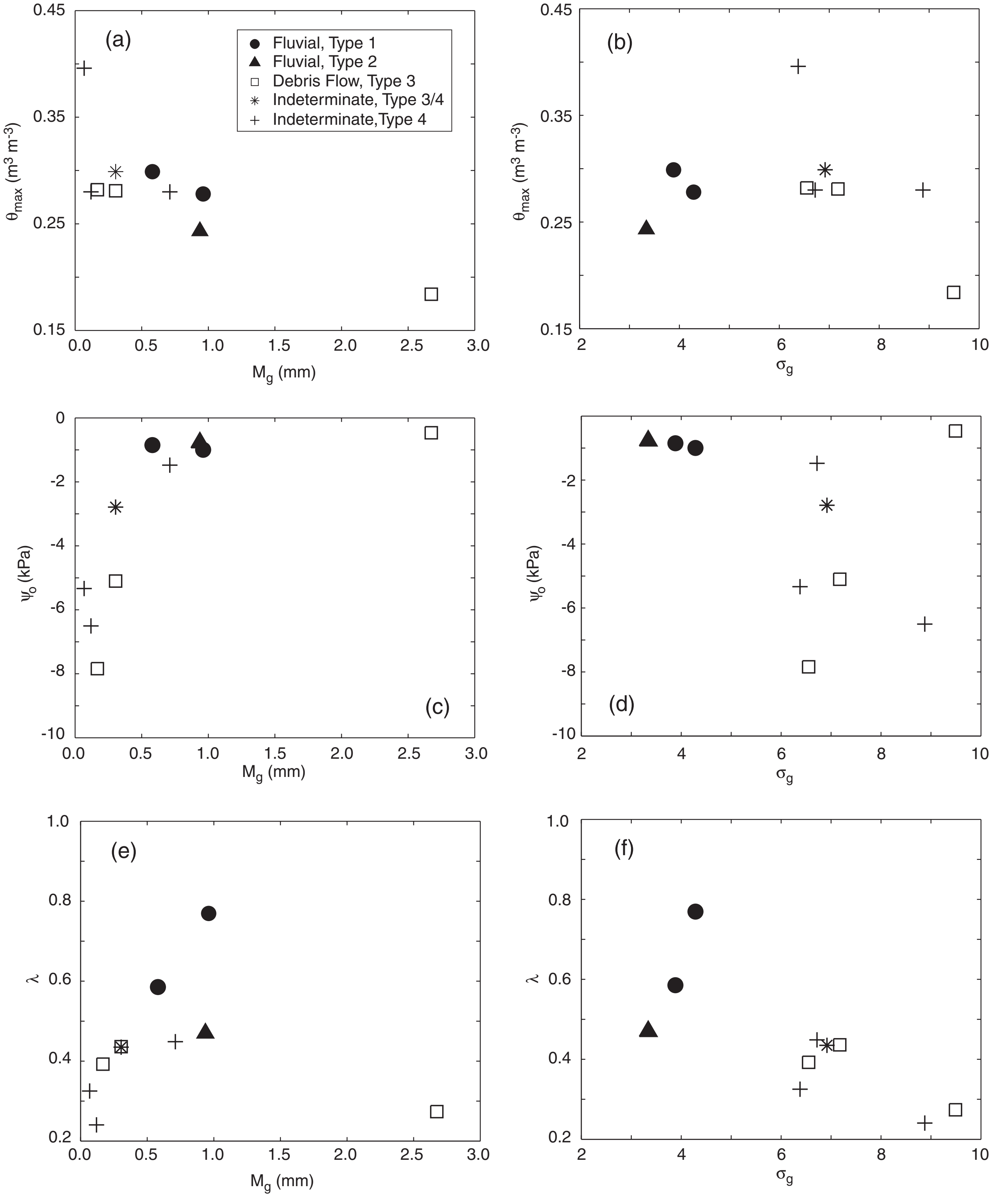

Fig. 7. Textural variables compared with maximum water content (θ_{max}) and Rossi–Nimmo (1994) fit parameters (scaling parameter for water potential, ψ_o; curve-shape parameter, λ). Scatter plots show comparisons with (a, c, e) geometric mean particle diameter (M_g) and (b, d, f) geometric standard deviation (σ_g), for n = 10 samples. Symbols indicate sample categories of Fig. 3, with results for individual samples listed in Table 3. Solid symbols represent fluvial samples and open symbols represent debris flow samples.

The θ_{max} value increases with decreasing M_g (Fig. 7a), but shows no clear trend with σ_g (Fig. 7b), even though one might expect θ_{max} to decrease with greater σ_g, as small particles infill voids near large particles. Samples classified as fluvial do not have consistently greater θ_{max} values than debris flow samples, as suggested by Fig. 1.

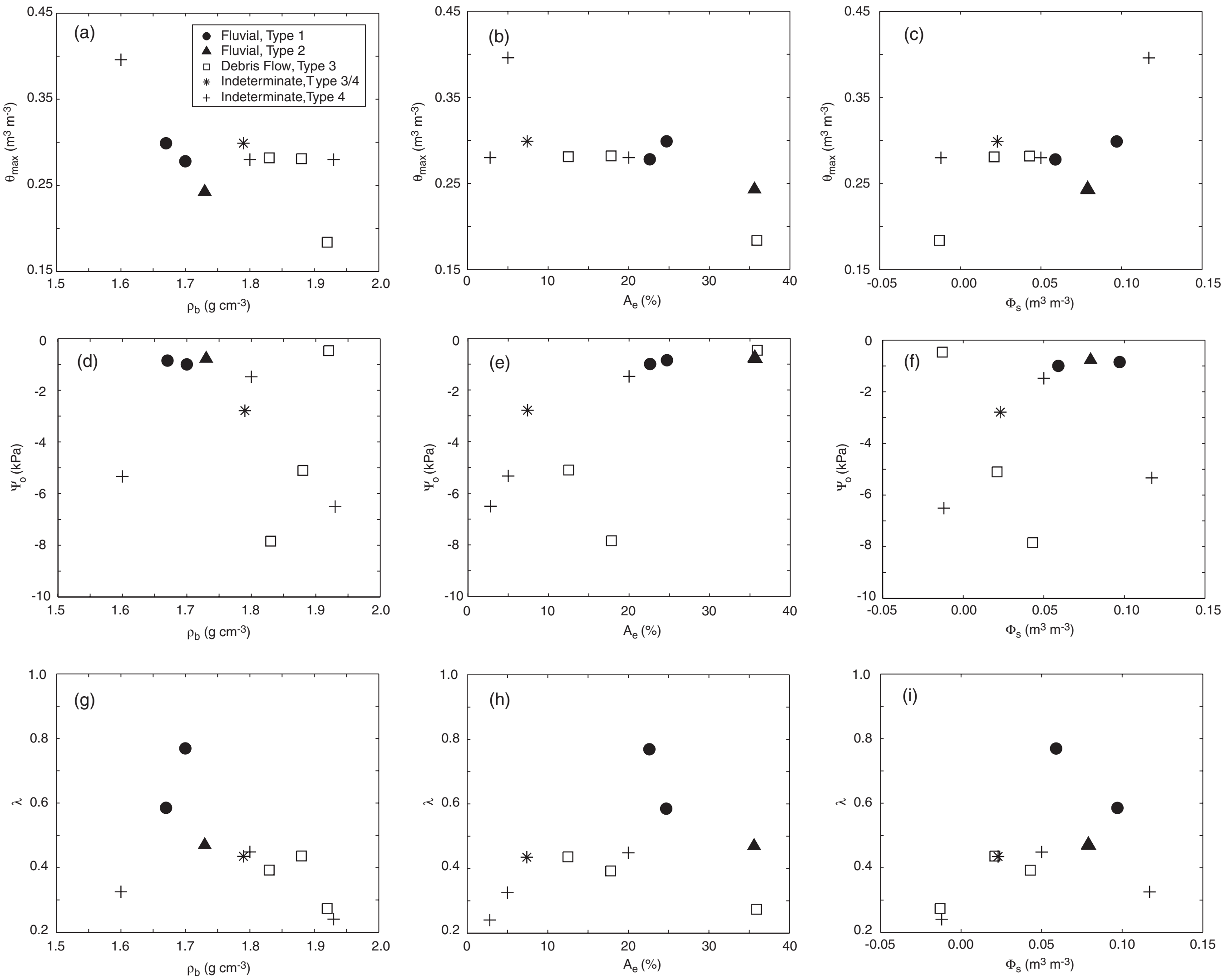

Fig. 8. Structural variables compared with maximum water content (θ_{max}) and Rossi–Nimmo (1994) fit parameters (ψ_o and λ). Scatter plots show comparisons with (a, d, g) bulk density (ρ_b); (b, e, h) trapped air fraction of porosity (A_e); and (c, f, i) porosity-based randomness index (Φ_s), for $n = 10$ samples. Symbols indicate sample categories of Fig. 3, with results for individual samples listed in Table 3. Solid symbols represent fluvial samples and open symbols represent debris flow samples.

The increase in θ_{max} with decreasing M_g is likely due to structural differences arising from "house of cards" stacking of platy minerals rather than from depositional sorting. Small particles in the SC Wash samples should be platy due to the muscovite-rich source rock.

The ψ_o parameter increases toward zero as M_g increases (Fig. 7c), consistent with known textural effects on $\theta(\psi)$. Samples classified as fluvial tend to have larger ψ_o values than debris flow samples, possibly due to a greater abundance of structure-related large pores. The fluvial samples, all with large M_g, also follow the general ψ_o vs. M_g (textural) trend of the entire data set. Smaller σ_g values for fluvial samples may create, on average, larger pores that effectively increase the ψ_o values. Figure 7d illustrates this effect: as σ_g increases, ψ_o usually decreases, suggesting a reduction of pore sizes from small particles occupying voids between large particles.

Greater λ values correspond to increased steepness of the middle range of the $\theta(\psi)$ curve. The correlation between λ and M_g is weak ($r = -0.032$, Table 4) overall, consistent with Miller and Miller (1956) similitude theory that a linear scaling of all particle and pore sizes of the medium would not affect λ. In one of the more strongly established trends, Fig. 7f shows that λ decreases as σ_g increases, indicating the spread in pore size correlates with the spread in particle size. This trend is consistent with a predominantly textural influence on $\theta(\psi)$, although scatter in the data may result in part from structural influences as well as measurement uncertainty.

The scatter plots (Fig. 7) and correlation coefficients (Table 4) show that the $\theta(\psi)$ parameters (θ_{max}, ψ_o, and λ) are, as expected, influenced by texture, represented by M_g or σ_g. Of these parameters, M_g strongly affects θ_{max} and ψ_o, while σ_g strongly affects λ. Structural influences are suggested, however, in that the fluvial samples have consistently larger (closer to zero) ψ_o values and larger λ values than nearly all other samples. Both of these structural trends are consistent with the hypotheses in

Table 4. Correlation coefficients between water retention parameters and indicators of texture or structure.

	Geometric mean particle diameter M_g	Geometric particle-size standard deviation σ_g	Bulk density ρ_b	Trapped air fraction of porosity A_e	Porosity-based randomness index Φ_s
Max. saturated water content, θ_{max}	−0.777**	−0.232	−0.662*	−0.716*	0.645*
Scaling parameter for water potential, ψ_o	0.663*	−0.384	−0.247	0.713*	0.156
Shape parameter, λ	−0.032	−0.776**	−0.519	0.289	0.438
M_g	1	0.221	0.281	0.778**	−0.338
σ_g		1	0.754*	−0.334	−0.778**
ρ_b			1	−0.006	−0.955***
A_e				1	0.060
Φ_s					1

* Significant at the 0.05 level of probability.
** Significant at the 0.01 level of probability.
*** Significant at the 0.001 level of probability.

Fig. 1. Textural influences on the fluvial samples are also evident; these samples, in general, have larger M_g values and are better sorted (with smaller σ_g values) than the debris-flow samples. Structural influence on the fluvial samples is suggested by data in Table 2; on average, A_e values were 28% for fluvial samples and 22% for debris-flow samples. This difference goes in the expected direction if greater variation in pore size correlates with greater air trapping, but a larger data set is needed to establish the significance of this trend.

This study's second objective, quantifying structural differences, would ideally be accomplished by comparing samples with identical PSDs. The PSDs of samples in this study vary too much for this objective to be accomplished through direct comparison, but structure may be evaluated in terms of A_e or Φ_s values.

The relations among the $\theta(\psi)$ parameters (θ_{max}, ψ_o, and λ) and the structural parameters (ρ_b, A_e, and Φ_s) are shown in Fig. 8. As expected, and to a large extent required for self-consistency, θ_{max} tends to decrease with increasing ρ_b and A_e and tends to increase with Φ_s. Among these, A_e most strongly correlates with θ_{max} ($r = -0.716$; Table 4). The strong correlation of Φ_s with ρ_b ($r = -0.955$) is necessary by definition, and thus not of interest. Although trends for ψ_o are less clear, ψ_o most strongly correlates with A_e ($r = 0.713$), increasing toward zero as A_e increases (Fig. 8e). Values of λ decrease with smaller ρ_b ($r = -0.519$), but have no clear trends for A_e or Φ_s.

The fluvial samples SC-2, OG-1, and OG-2 have greater A_e values than all other samples except the coarsest sample, OGL-1 11.5, suggesting structural influences that are not obvious from Fig. 7 and 8, and that accord with the hypothetical relationships in Fig. 1. The fluvial samples had larger Φ_s values than all other samples except SCF 57, also consistent with the expected structural trends.

Regression Analysis

Multiple linear-regression analyses were conducted to determine which of the textural and structural parameters were best able to explain the variation in the hydraulic parameters. The "all possible subsets" approach (Draper and Smith, 1981; Rawlings et al., 1998) was used to determine the best set of explanatory variables (among M_g, σ_g, ρ_b, A_e, and Φ_s) for estimating each of the three hydraulic parameters (θ_{max}, ψ_o, and λ). All possible multiple linear-regression equations involving the potential explanatory variables are computed (for $2^m - 1$ equations, where m is the maximum number of potential explanatory variables, i.e., $m = 5$ in our application), and statistics such as the coefficient of determination (R^2), adjusted R^2 (R^2_{adj}), residual mean square, and Mallow's C_p are evaluated. Results are grouped according to the number of variables in the equation (p) and ordered from highest to lowest R^2. The candidates for "best" model typically have the highest R^2 per p variable subset. Mallow's C_p suggests the best subset of explanatory variables for each response variable, by comparing computed C_p values to the criterion of $C_p = p + 1$. Values of $C_p < p + 1$ (i.e., $\Delta C_p = C_p - p - 1$ is negative) indicate that the model is overspecified, or that more explanatory variables are included in the regression variate than are necessary to fit the data.

Multiple linear-regression analyses were conducted using custom programs written with Matlab (The MathWorks, Inc., Version 6, Release 12) and the Statistics Toolbox utility. In Table 5, the set of explanatory variables with the highest R^2 is shown for each p variable subset. The best subset for each of the parameters θ_{max}, ψ_o, and λ (underlined in Table 5) had a calculated C_p value closest to the criterion $p + 1$ while preserving the smallest number of explanatory variables. For θ_{max}, the best model occurred for $p = 3$, and included A_e, Φ_s, and σ_g. For ψ_o, the best model was for $p = 2$, and included M_g and σ_g. This model was slightly overspecified (calculated $C_p = 1.56 < p + 1 = 3$). Although C_p for the four-variable model was closest to the C_p criterion ($\Delta C_p = 0.88$), this model was not chosen because the slight improvement in fit it may have offered was insufficient to justify the use of two more explanatory variables. For λ, the best subset involved σ_g only.

Some ambiguity in the use of C_p for selecting the best subset is often encountered in the approach using all possible regressions. However, an alternative approach, backward elimination of variables, produced the same best subsets of explanatory variables for θ_{max}, ψ_o, and λ. Backward elimination starts from the complete set of explanatory variables, with subsequent removal of variables (one at a time) until an optimum variate is achieved. Removing a variable requires testing whether any of the partial t values of the coefficients for the

Table 5. Stepwise regression results.

Response variable	p†	R^2	C_p‡	F	Explanatory variables
θ_{max}	1	0.604	707.02	12.22**	M_g
	2	0.987	18.80	273.11***	A_e, Φ_s
	3§	0.996	4.71	535.07***	A_e, Φ_s, σ_g
	4	0.998	4.00	561.84***	ρ_b, A_e, Φ_s, σ_g
	5	0.998	6.00	359.60***	ρ_b, A_e, Φ_s, M_g, σ_g
ψ_o	1	0.508	4.33	8.27*	A_e
	2	0.735	1.56	9.72**	M_g, σ_g
	3	0.793	2.34	7.68*	A_e, M_g, σ_g
	4	0.804	4.12	5.11	ρ_b, A_e, M_g, σ_g
	5	0.810	6.00	3.40	ρ_b, A_e, Φ_s, M_g, σ_g
λ	1	0.602	1.64	12.09**	σ_g
	2	0.671	2.31	7.14*	Φ_s, σ_g
	3	0.761	2.59	6.36*	ρ_b, Φ_s, σ_g
	4	0.791	4.00	4.74	ρ_b, A_e, M_g, σ_g
	5	0.791	6.00	3.04	ρ_b, A_e, Φ_s, M_g, σ_g

* Significant at the 0.05 level of probability.
** Significant at the 0.01 level of probability.
*** Significant at the 0.001 level of probability.
† Number of explanatory variables in model, excluding intercept term.
‡ Mallow's C_p statistic is computed from $2(p + 1) - n + \frac{SSQ_{res}}{s^2}$, where n is the number of observations, SSQ_{res} is the residual sum of squares for the p variable model being tested, and s^2 is an estimate of the population variance (calculated from the p variable model containing all possible variables). The C_p value of a particular subset that most closely approaches the criterion $C_p = p + 1$ may indicate the "best" subset of x variables. Values of $C_p < p + 1$ indicate model overspecification.
§ Underlined values indicate the "best" subset selected for θ_{max}, ψ_o, and λ.

variables in the regression variate are significantly different from zero. The partial t value is calculated by dividing the coefficient determined for each explanatory variable during the regression process by its standard error. The variable whose partial t value is the lowest is removed from the regression equation, and a new regression equation is developed from the smaller subset of explanatory variables. For θ_{max}, M_g was the first variable removed using backward elimination, followed by ρ_b. For ψ_o, the first variable eliminated was Φ_s, followed by ρ_b and A_e. For λ, the variables were eliminated in the following order until σ_g was left as the only significant variable: Φ_s, ρ_b, A_e, M_g. The coefficients for the explanatory variables included in the best regression equations for θ_{max}, ψ_o, and λ were all significantly different from zero at a significance level of 0.05.

For θ_{max}, examination of the goodness of fit of the models in the regression analysis allows further interpretation of the trends noted above, that correlation is strongest with M_g, ρ_b, A_e, and Φ_s. The trend with M_g is noteworthy because of its fundamental independence of θ_{max}. Regression analysis shows that although M_g (R^2 = 0.604) is the best choice for a one-variable model of θ_{max}, fit improved as much as 39% for the two- and three-variable models that included A_e, Φ_s, and σ_g. The correlations with A_e and Φ_s must be discounted because θ_{max} is arithmetically determined by these parameters, although other structural indicators not used in this study may have predictive value.

For ψ_o, which correlated most strongly with A_e followed by M_g (Table 4), the one-variable model included A_e, although the variation was best explained by the combination of textural parameters M_g and σ_g, with $R^2 = 0.735$. The addition of A_e in the equation for $p = 3$ improved the model fit by 6%. The strong collinearity between M_g and A_e (r = 0.778), however, makes this model less desirable than the one involving only M_g and σ_g. Overall, these results suggest that structural information implicit in A_e has value in a PTM.

For λ, which correlated most strongly with σ_g, a one-variable model involving σ_g best explained the variation in λ (R^2 = 0.602). Adding more variables provided only slight improvements in model fit and overspecified the model by the C_p criterion, even though the R^2 was only 0.602 for p = 1.

Although the data set is small, regression results suggest that in addition to textural information, structural indicators may be useful as explanatory variables to predict $\theta(\psi)$. Most noteworthy is the potential value of A_e for explaining the variation in ψ_o. Independent determination of A_e (e.g., from field studies) may prove useful for estimating θ_{max}.

SUMMARY AND CONCLUSIONS

Property-transfer models are generally based more strongly on textural than on structural indicators, and are often considered to work best in media composed primarily of randomly arranged particles, as frequently is true of sands. We explored the validity of these generalizations and the possible benefits of incorporating structural indicators into PTMs for the case of structural influences deriving from the mode of sediment deposition. Because of systematic differences in particle arrangement arising from distinct depositional processes, investigation of structural effects due to deposition is simpler and in some ways more instructive than those due to aggregation or biotic processes. For this evaluation we measured water retention [$\theta(\psi)$] curves on 10 undisturbed core samples from washes in the western Mojave Desert. Samples were categorized as originating from fluvial or debris flow environments by analyzing the stratigraphy of the cores and by comparing σ_g for the bulk sample. Textural (M_g and σ_g) and structural (ρ_b, A_e, and Φ_s) parameters were used as candidate explanatory variables in parameter-correlation and multiple linear-regression analyses to evaluate possible improvements in predictions of $\theta(\psi)$ parameters (θ_{max}, ψ_o, and λ) over texture-based PTMs.

Texture had greater influence than structure on the $\theta(\psi)$ properties of our samples. Values of θ_{max} and ψ_o correlated strongly with M_g ($r = -0.777$ and $r = 0.663$, respectively), whereas λ correlated best with σ_g ($r = -0.776$). Values of ψ_o correlated strongly with the structural indicator A_e (r = 0.713), and λ correlated weakly with all of the structural indicators ($r < |-0.519|$). Most A_e values exceeded the general guideline of 10% and correlated significantly with texture, being greater for coarser material.

Other evidence of structural influence is apparent in that debris flow samples generally had smaller Φ_s and A_e; the three fluvial samples ranked in the four highest values of both Φ_s and A_e. Smaller Φ_s indicates a more random structure (Nimmo, 1997), which is expected from the more rapid, disorderly deposition of debris flows. Smaller A_e may correlate with a narrower pore-size distribution (Orlob and Radhakrishna, 1958; Bond and Collis-George, 1981), likewise a probable characteristic of debris flows. For predictions, the best one-variable model for ψ_o was based on A_e ($R^2 = 0.508$), although the best ψ_o model overall involved M_g and σ_g ($R^2 = 0.735$). While the evidence in this study indicates only a slight influence of structure on $\theta(\psi)$, it should be noted that structure-affecting mechanisms associated with differences in depositional environment (Fig. 1) are subtle compared with those associated with aggregation and macropores.

The development of more general and improved PTMs that can be applied to multiple sites, and that are based on theoretical relationships between the bulk physical and hydraulic properties, will benefit from improved knowledge of structural effects, perhaps quantified by A_e, Φ_s, or related parameters. Further work might explore the influence of structural mechanisms such as that of smaller particles infilling large pores next to large particles (for randomly structured media like debris-flow deposits). While not precluding the role of texture as the primary basis for PTMs for sandy media, we have shown that supplemental use of the simple structural indicators A_e and Φ_s can improve PTM predictions.

ACKNOWLEDGMENTS

The authors thank the Mojave Water Agency for providing funding for the initial phase of this study.

REFERENCES

Andraski, B.J. 1996. Properties and variability of soil and trench fill at an arid waste-burial site. Soil Sci. Soc. Am. J. 60:54–66.

Arya, L.M., and J.F. Paris. 1981. A physicoempirical model to predict the soil moisture characteristic from particle-size distribution and bulk density data. Soil Sci. Soc. Am. J. 45:1023–1030.

Beyer, W.H. 1991. CRC standard mathematical tables and formulae. 29th ed. CRC Press, Inc., Boca Raton, FL.

Blake, G.R., and K.H. Hartge. 1986. Particle density. p. 378–379. *In* A. Klute (ed.) Methods of soil analysis. Part 1. 2nd ed. Agron. Monogr. 9. ASA and SSSA, Madison, WI.

Bond, W.J., and N. Collis-George. 1981. Ponded infiltration into simple soil systems: 1. The saturation and transition zones in the moisture content profiles. Soil Sci. 131:202–209.

Bouma, J. 1989. Using soil survey data for quantitative land evaluation. p. 177–213. *In* Advances in soil science. Vol. 9. Springer-Verlag, New York.

Campbell, G.S. 1985. Soil physics with BASIC–transport models for soil–plant systems. Elsevier, New York.

Campbell, G.S., and S. Shiozawa. 1992. Prediction of hydraulic properties of soils using particle-size distribution and bulk density data. *In* M.Th. van Genuchten et al. (ed.) International workshop on indirect methods for estimating the hydraulic properties of unsaturated soils, Riverside, CA. 11–13 Oct. 1989. Univ. of California, Riverside.

Constantz, J., W.N. Herkelrath, and F. Murphy. 1988. Air encapsulation during infiltration. Soil Sci. Soc. Am. J. 52:10–16.

Croney, D., and J.D. Coleman. 1954. Soil structure in relation to soil suction (pF). J. Soil Sci. 5:75–84.

Davidson, J.M., D.R. Nielsen, and J.W. Biggar. 1966. The dependence of soil water uptake and release upon the applied pressure increment. Soil Sci. Soc. Am. Proc. 30:298–304.

Dorsey, N.E. 1940. Properties of ordinary water-substance. Hafner Publishing Company, New York.

Draper, N.R., and H. Smith. 1981. Applied regression analysis. 2nd ed. John Wiley & Sons, New York.

Elrick, D.E., and C.B. Tanner. 1955. Influence of sample pretreatment on soil moisture retention. Soil Sci. Soc. Am. Proc. 19:279–282.

Faybishenko, B.A. 1995. Hydraulic behavior of quasi-saturated soils in the presence of entrapped air: Laboratory experiments. Water Resour. Res. 31:2421–2435.

Fayer, M.J., and D. Hillel. 1986. Air encapsulation: I. Measurement in a field soil. Soil Sci. Soc. Am. J. 50:568–572.

Folk, R.L. 1980. Petrology of sedimentary rocks. 2nd ed. Hemphill Publishing Company, Austin, TX.

Gee, G.W., M.D. Campbell, G.S. Campbell, and J.H. Campbell. 1992. Rapid measurement of low soil water potentials using a water activity meter. Soil Sci. Soc. Am. J. 56:1068–1070.

Gee, G.W., and D. Or. 2002. Particle-size analysis. p. 255–293. *In* J.H. Dane and G.C. Topp (ed.) Methods of soil analysis. Part 4. SSSA Book Ser. 5. SSSA, Madison, WI.

Greacen, E.L., G.R. Walker, and P.G. Cook. 1987. Evaluation of the filter paper method for measuring soil water suction. Int. Conf. Measur. Soil Plant Water Status 1:137–143.

Gregson, K., D.J. Hector, and M. McGowan. 1987. A one-parameter model for the soil water characteristic. J. Soil Sci. 38:483–486.

Gupta, S.C., and W.E. Larson. 1979. Estimating soil water retention characteristics from particle size distribution, organic matter content, and bulk density. Water Resour. Res. 15:1633–1635.

Haverkamp, R., and J.Y. Parlange. 1986. Predicting the water-retention curve from particle-size distribution. 1. Sandy soils without organic matter. Soil Sci. 142(6):325–339.

Haverkamp, R., and P. Reggiani. 2002. Physically based water retention prediction models. p. 762–777, 781–782. *In* J.H. Dane and G.C. Topp (ed.) Methods of soil analysis. Part 4. SSSA Book Ser. 5. SSSA, Madison, WI.

Izbicki, J.A., P. Martin, and R.L. Michel. 1995. Source, movement, and age of groundwater in the upper part of the Mojave River Basin, California, U.S.A. p. 43–56. *In* E.M. Adar and C. Leibundgut (ed.) Application of tracers in arid zone hydrology. Publ. 232. International Association of Hydrological Sciences.

Izbicki, J.A., R.L. Michel, and P. Martin. 1998. Chloride and tritium concentrations in a thick unsaturated zone underlying an intermittent stream in the Mojave Desert, southern California, U.S.A. p. 81–88. *In* J.V. Brahana et al. (ed.) Gambling with groundwater—Physical, chemical, and biological aspects of aquifer-stream relations. Proceedings of the joint meeting of the XXVIII Congress of the International Association of Hydrogeologists and the annual meeting of the American Institute of Hydrologists, Las Vegas, NV. 28 Sept.–2 Oct. AIH, Smyrna, GA.

Izbicki, J.A. 1999. Transition probability/Markov chain analysis of the subsurface geology of the Victorville fan in the western part of the Mojave Desert, Southern California. p. 55–64. *In* R.E. Reynolds and J. Reynolds (ed.) Tracks along the Mojave, Quarterly of the San Bernardino County Museum Association. Vol. 46.

Izbicki, J.A., D.A. Clark, M.I. Pimentel, M. Land, J. Radyk, and R.L. Michel. 2000. Data from a thick unsaturated zone underlying Oro Grande and Sheep Creek Washes in the western part of the Mojave Desert, near Victorville, San Bernardino County, California. Open-File Rep. 00-262. USGS, Sacramento, CA.

Jayawardane, N.S., and S.A. Prathapar. 1992. Effect of soil loosening on the hydraulic properties of a duplex soil. Aust. J. Soil Res. 30:959–975.

Krumbein, W.C. 1938. Size frequency distributions of sediments and the normal phi curve. J. Sediment. Petrol. 8(3):84–90.

Lin, H.S., K.J. McInnes, L.P. Wilding, and C.T. Hallmark. 1999a. Effects of soil morphology on hydraulic properties: I. Quantification of soil morphology. Soil Sci. Soc. Am. J. 63:948–954.

Lin, H.S., K.J. McInnes, L.P. Wilding, and C.T. Hallmark. 1999b. Effects of soil morphology on hydraulic properties: II. Hydraulic pedotransfer functions. Soil Sci. Soc. Am. J. 63:955–961.

Mecke, M., C.J. Westman, and H. Ilvesniemi. 2002. Water retention capacity in coarse podzol profiles predicted from measured soil properties. Soil Sci. Soc. Am. J. 66:1–11.

Meisling, K.E., and R.E. Weldon. 1989. Late Cenozoic tectonics of the northwestern San Bernardino Mountains, southern California. Geol. Soc. Am. Bull. 101:106–128.

Miller, D.M., and D.R. Bedford. 2000. Geologic map database of the

El Mirage Lake area, San Bernardino and Los Angeles counties, California. Open-File Rep. 00-0222. USGS, Reston, VA.

Morton, D.M., and P.M. Sadler. 1989. The failings of the Pelona Schist: Landslides and sackungen in the Lone Pine Canyon and the Wrightwood areas of the San Gabriel Mountains of Southern California. p. 301–322. *In* P.M. Sadler and D.M. Morton (ed.) Landslides in a semiarid environment with emphasis on the inland valleys of southern California. Vol. 2. Publications of the Inland Geological Society.

Miller, E.E., and R.D. Miller. 1956. Physical theory for capillary flow phenomena. J. Appl. Phys. 27:324–332.

Mualem, Y. 1974. A conceptual model of hysteresis. Water Resour. Res. 10:514–520.

Nimmo, J.R. 1997. Modeling structural influences on soil water retention. Soil Sci. Soc. Am. J. 61:712–719.

Nimmo, J.R., and K.C. Akstin. 1988. Hydraulic conductivity of a sandy soil at low water content after compaction by various methods. Soil Sci. Soc. Am. J. 52:303–310.

Orlob, G.T., and G.N. Radhakrishna. 1958. The effects of entrapped gas on the hydraulic characteristics of porous media. Trans. Am. Geophys. Union 39:648–659.

Perkins, K.S. 2003. Measurement of sedimentary interbed hydraulic properties and their hydrologic influence near the Idaho Nuclear Technology and Engineering Center at the Idaho National Engineering and Environmental Laboratory. Water Resour. Invest. Rep. 03-4048. USGS, Reston, VA.

Pettijohn, F.J. 1975. Sedimentary rocks. 3rd ed. Harper & Row, New York.

Puckett, W.E., J.H. Dane, and B.F. Hajek. 1985. Physical and mineralogical data to determine soil hydraulic properties. Soil Sci. Soc. Am. J. 49:831–836.

Rawlings, J.O., S.G. Pantula, and D.A. Dickey. 1998. Applied regression analysis: A research tool. 2nd ed. Springer-Verlag, Inc., New York.

Rawls, W.J., and D.L. Brakensiek. 1982. Estimating soil water retention from soil properties. J. Irrig. Drainage Div., Proc. ASCE 108 (IR2):166–171.

Rawls, W.J., and Y.A. Pachepsky. 2002. Soil consistence and structure as predictors of water retention. Soil Sci. Soc. Am. J. 66: 1115–1126.

Ross, P.J., J. Williams, and K.L. Bristow. 1991. Equation for extending water-retention curves to dryness. Soil Sci. Soc. Am. J. 55: 923–927.

Rossi, C., and J.R. Nimmo. 1994. Modeling of soil water retention from saturation to oven dryness. Water Resour. Res. 30:701–708.

Rossi, C., and J.R. Nimmo. 1996. Modelli modificati di curve di ritenzione idrica in mezzi porosi non saturi. Quaderni di Geologia Applicata 3(2):127–136.

Saxton, K.E., W.J. Rawls, J.S. Romberger, and R.I. Papendick. 1986. Estimating generalized soil-water characteristics from texture. Soil Sci. Soc. Am. J. 50:1031–1036.

Schaap, M.G., F.J. Leij, and M.T. van Genuchten. 1998. Neural network analysis for hierarchical prediction of soil hydraulic properties. Soil Sci. Soc. Am. J. 62:847–855.

Scheinost, A.C., W. Sinowski, and K. Auerswald. 1997. Regionalization of soil water retention curves in highly variable soilscape. I. Developing a new pedotransfer function. Geoderma 78:129–143.

Sharp, R.P., and L.H. Nobles. 1953. Mudflow of 1941 at Wrightwood, southern California. Geol. Soc. Am. Bull. 64:547–560.

Soil Survey Staff. 1975. Soil taxonomy: A basic system of soil classification for making and interpreting soil surveys. USDA-SCS Agric. Handb. 436. U.S. Gov. Print. Office, Washington, DC.

SSSA. 1997. Glossary of soil science terms. SSSA, Madison, WI.

Tomasella, J., Y.A. Pachepsky, S. Crestana, and W.J. Rawls. 2003. Comparison of two techniques to develop pedotransfer functions for water retention. Soil Sci. Soc. Am. J. 67:1085–1092.

Vereecken, H., J. Maes, J. Feyen, and P. Darius. 1989. Estimating the soil moisture retention characteristic from texture, bulk density, and carbon content. Soil Sci. 148(6):389–403.

Weldon, R. 1985. Implications of the age and distribution of the late Cenozoic stratigraphy in Cajon Pass, southern California. p. 59–68. *In* R.E. Reynolds (ed.) Geologic investigations along Interstate 15; Cajon Pass to Manix Lake, California. San Bernardino County Museum, Redlands, CA.

Winfield, K.A. 2000. Factors controlling water retention of alluvial deposits, western Mojave Desert. Master's thesis, San Jose State Univ., San Jose.

Winfield, K.A., and J.R. Nimmo. 2002. Controlled liquid-volume [water retention and storage]. p. 698–703, 717–720. *In* J.H. Dane and G.C. Topp (ed.) Methods of soil analysis, Part 4. SSSA Book Ser. 5. SSSA, Madison, WI.

Wösten, J.H.M., and M.Th. van Genuchten. 1988. Using texture and other soil properties to predict the unsaturated soil hydraulic functions. Soil Sci. Soc. Am. J. 52:1762–1770.